ELSEVIER

Journal of Alloys and Compounds 271–273 (1998) 610–615

Journal of ALLOYS AND COMPOUNDS

Phase characterisation of simulated high burn-up UO_2 fuel

J. Cobos*, D. Papaioannou, J. Spino, M. Coquerelle

European Commission, Joint Research Centre, Institute for Transuranium Elements, Postfach 2340, D-76125 Karlsruhe, Germany

Abstract

To determine the lattice constant variation with burn-up and the oxidation behaviour at high temperatures, simulated UO_2-spent fuels with burn-ups up to 200 GWd tM^{-1} were prepared by cold pressing and sintering and characterised by X-ray diffraction analysis and thermogravimetry. The fcc-lattice parameter of the sintered samples determined at room temperature, showed a continuous decrease with the simulated burn-up. During oxidation the conversion of the simulated fuels to the $(U,FP)_4O_9$ and $(U,FP)_3O_8$-type phases was strongly delayed when the simulated burn-up exceeded 80 GWd tM^{-1}. Also, at high burn-ups (>100 GWd tM^{-1}), large fractions of the $(U,FP)_4O_9$-type phase remained untransformed to $(U,FP)_3O_8$ after prolonged exposure to air at 950–1000°C. This suggests a marked widening of the $(U,FP)_4O_9$-phase field when the amount of substituted uranium atoms exceeds values of about 8%. © 1998 Elsevier Science S.A.

Keywords: Simulated spent fuel; Oxidation; Lattice parameter; High temperature

1. Introduction

More than 30 fission product elements are formed during the irradiation of nuclear fuels, whose final amounts depend on various parameters, mainly type and concentrations of fissile atoms, specific power, neutron energy, irradiation time and cooling time. Post-irradiation examinations of UO_2 fuels have shown that the non-volatile fission products are basically distributed in three phases, namely the lanthanides and partially Zr dissolved in the fcc-matrix, Mo and the noble metals in the metallic (five-metal particles) precipitates and Ba and partially Zr in the ceramic (Perovskite-type) precipitates [1,2].

Up to burn-ups of about 80 GWd tM^{-1}, several studies have shown that simulated spent fuels present analogous phase characteristics to the irradiated fuels [3–5]. Due to the present trend in LWR fuels of increasing the average burn-up to 60–70 GWd tM^{-1}, with peak burn-ups at the pellet-rim region of about 2.5 times the average [6], extension of the available data on simulated spent fuels up to burn-ups of about 200 GWd tM^{-1} is necessary.

Under normal irradiation conditions, post-irradiation studies of LWR fuels performed at ITU, indicate that no new matrix phases are formed at high burn-ups, only an increase of the amount of the above mentioned precipitates (predominantly of the metallic ones) at the fuel periphery is noticed [7]. Thus, under normal irradiation conditions, the main effect expected at high burn-ups in the fuel matrix is a larger decrease of its lattice parameter.

However, under oxidative conditions, as they may be caused by accidental cladding breaches during service or after fuel discharge, a different phase behaviour of the high burn-up fuel is expected. In fact, low-temperature oxidation studies of irradiated [8] and simulated fuels [9] up to 40 GWd tM^{-1} have shown a reduced transformation rate to the U_3O_8-type phase as burn-up increases. Similar results were obtained for unirradiated Gd_2O_3–UO_2 solid solutions [8]. The proposed reason for this behaviour had been the stabilisation of the U_4O_9-type phase by dissolved elements in the uranium oxide lattice.

In the present work, extension of the data on simulated UO_2-spent fuels up to 200 GWd tM^{-1} will be given, including the lattice parameter determination at room temperature after reducing sintering and the oxidation kinetics in air up to temperatures of 950–1000°C. Based on these data, additional evidence of a marked oxidation stagnation above 100 GWd tM^{-1} will be provided.

2. Experimental

2.1. Composition of the simulated UO_2 fuels

Compositions of fission products and actinides for a typical LWR fuel with initial enrichment of 3.5% U^{235}

*Corresponding author. Tel.: +49 7247 951548; fax: +49 7247 951593; E-mail: cobos@e-mail.tui.fzk.de

PII: S0925-8388(98)00170-4

were calculated with the computer code ORIGEN [10]. Mean power assumed was 15.2 MW tMU^{-1} for a postulated neutron flux of 2.02×10^{13} n cm^{-2} s^{-1}. The burn-up range selected was 25–195 GWd tM^{-1}. The compositions of some fuels used for this study are shown in Table 1. Elements within brackets were replaced by the head element of the line according to their atomic concentrations. Kr, Xe and I are not included.

2.2. Sample preparation

Homogeneous mixtures of stoichiometric UO_2 powder and simulated fission product compounds were prepared by planetary ball-milling for 24 h in alcoholic media, according to Table 1. After drying, prereaction of the mixtures was done at 950°C in an Ar-stream over 24 h. After granulation, pelletization of powders was done by uniaxial compaction to about 60% green density, and addition of zinc-stearate as lubricant. Pellets were sintered to high density by heat-treatment in Ar/H_2 (6%) atmosphere over 32 h at 1640°C, after a previous short-hold at 400°C to remove the zinc-stearate. No microcracking of the pellets was observed by scanning electron microscopy.

2.3. X-ray diffraction analysis

X-ray diffraction patterns of UO_2 and simulated fuels after sintering were obtained by means of a θ/θ Seifert diffractometer with Ni filtered Cu Kα radiation. Samples were examined in the as-sintered condition (bulk-pellets) and after crushing (powder ≠220-mesh). For the pellet samples, surface polishing with 400 grid SiC paper was done. Diffraction angle range analysed was $10°<\theta<82°$, using the step-scanning mode with 0.08–0.15° step-widths. (3°)/divergence(2°) and anti-scatter(1°)/receiving(0.5°) slits were used for the incident and diffracted beams respectively. Background stripping and profile fitting programs [11] were used to determine the $K\alpha_1$ peak positions. Systematic peak shiftings were corrected using Si-(NIST 640b) as external standard. After this correction, the lattice parameters were determined by extrapolation of the curves a (*hkl*) vs. cos θ/tan θ to $\theta=90°$. Repeated measurements of the same material (renewed sample preparation) revealed an accuracy of $\pm1\times10^{-5}$ nm in the unit-cell determinations.

Table 1
ORIGEN code calculation of the simulated spent fuels

Element	%wt metal				
	Burn-up [GWd tM^{-1}]				
	25	70	115	150	200
Code calculations					
Ce (Ce, Np, Pu)	0.71	1.33	1.70	1.96	2.31
La (La, Am, Cm)	0.09	0.32	0.61	0.81	1.15
Rb	0.03	0.06	0.09	0.11	0.14
Sr	0.07	0.15	0.21	0.26	0.33
Zr	0.34	0.70	1.03	1.31	1.71
Mo	0.29	0.71	1.13	1.47	1.97
Ru (Tc)	0.26	0.69	1.22	1.59	2.07
Rh	0.04	0.07	0.08	0.08	0.09
Pd	0.06	0.42	0.86	1.19	1.75
Ag	0.01	0.02	0.03	0.03	0.04
Cd	0.00	0.04	0.11	0.17	0.29
Te	0.04	0.10	0.17	0.22	0.30
Cs	0.24	0.53	0.82	1.04	1.37
Ba	0.12	0.35	0.57	0.78	1.08
Pr	0.11	0.23	0.34	0.44	0.56
Pm (Nd)	0.32	0.85	1.35	1.76	2.74
Sm	0.06	0.15	0.21	0.24	0.27
Gd (Eu)	0.01	0.10	0.24	0.36	0.65
U	97.16	93.10	89.12	86.04	81.01

2.4. Thermogravimetric measurements

The oxidation kinetics of the simulated fuels, as well as a control reference curve for UO_2, were determined by thermogravimetry using a Netzsch-STA 409 thermoanalyzer. The estimated error in the measured O/M ratios, as governed by the reproducibility of repeated measurements under identical conditions, was estimated to be about ±0.005.

Just as for the X-ray diffraction analysis two oxidation series were performed, namely one with bulk sintered-pellets and another with pulverised pellets after sieving the powder through a ≠220-mesh. This led in all cases to an upper powder particle size of about 60 μm. The particle-size distribution measured by sedimentation was about 10 μm.

Before oxidation, equilibration of the samples at a reference O/M ratio of 2 ± 0.001 was performed by heating them at 850°C over 24 h under a gas mixture of $CO/CO_2=10$, with subsequent cooling to room temperature under the same atmosphere [12]. Then, oxidation of the samples was performed by heating them under flowing air (40 cm^3 min^{-1}) from 25°C to 1000°C at a linear heating rate of 1 K min^{-1}, under continuous weight-change monitoring.

3. Results

3.1. Composition determinations

The uranium concentration in the total mass of the simulated fuels after sintering was determined by coulometric titration. Table 2 shows comparison of these results with estimations based on the ORIGEN-2 calculations, assuming for the oxide the composition $U_{1-y}FP_yO_2$. The agreement between both measured and calculated concentrations lies within 0.1–0.3% (Table 2).

The distribution and content of the minor elements (FP) was studied by EMPA. Preliminary results indicate that Ce, La, Sr, Y, Pr and Nd are dissolved in the matrix, while Mo

Table 2
Comparison of measured and expected U-concentrations as function of the simulated burnup

Simulated	U-concentration in oxide (wt%)	
burnup (GWd tM^{-1})	Coulometric titration	ORIGEN-2 calculations (assuming $U_{1-y}FP_yO_2$)
25	85.5±0.1	85.36
60	82.1±0.1	82.42
70	81.6±0.1	81.38
90	80.0±0.1	79.87
115	77.6±0.1	77.53
135	76.5±0.1	75.81
150	74.9±0.1	74.56
165	73.7±0.1	74.56
185	71.8±0.1	71.62
200	70.4±0.1	69.80

and Ru are segregated as metal particles, and Ba and part of Zr as ceramic (grey-phase) precipitates. First quantitative results indicate an excess of Zr and Y in the fuel matrix, whose effect on the lattice constant measurements is discussed in Section 4.

3.2. Lattice parameter

Fig. 1 shows the measured lattice parameters of UO_2 and the simulated fuels as a function of burnup. For stoichiometric UO_2 the measured values were 0.54701±0.00001 nm for the pellet-sample and 0.54702±0.00001 nm for the powder-sample which is in agreement with the literature [13]. In Fig. 1 the data of other authors up to 90 GWd tM^{-1}, for simulated fuels [3–5,14] and for irradiated UO_2 [15] is shown. For the whole set of data, a well defined decreasing trend of the lattice parameters with increasing burnups is observed. However, it is noteworthy that below 90 GWd tM^{-1}, lower lattice constants were measured in this work in comparison with other literature data (Fig. 1). As discussed in Section 4, the reason for this behaviour is attributed to an excess of Zr and Y in our samples.

3.3. Oxidation behaviour

3.3.1. Powdered pellets

Typical oxidation curves of UO_2 and simulated spent fuel powders are shown in Fig. 2. Results are shown as weight-gain percentage versus temperature (Fig. 2). Conversion to O M^{-1} ratios is done via the formula $O/M=2+(\Delta W/W)\,M/16$, where W is the initial sample-weight and M the molecular weight of the oxide solid solution.

As confirmed by X-ray diffraction analysis, in the burn-up range 0–70 GWd tM^{-1}, the intermediate and final oxidation states ('plateaus') of the curves in Fig. 2 corresponded to the $(U, PF)_4O_9$ and $(U, FP)_3O_8$ structures. No formation of the U_3O_7-type tetragonal phase was observed, as confirmed by the lack of peak splitting at the typical reflections 200 (002) and 311 (113) [16,17]. In the highest burn-up range (≥127 GWd tM^{-1}), however, the

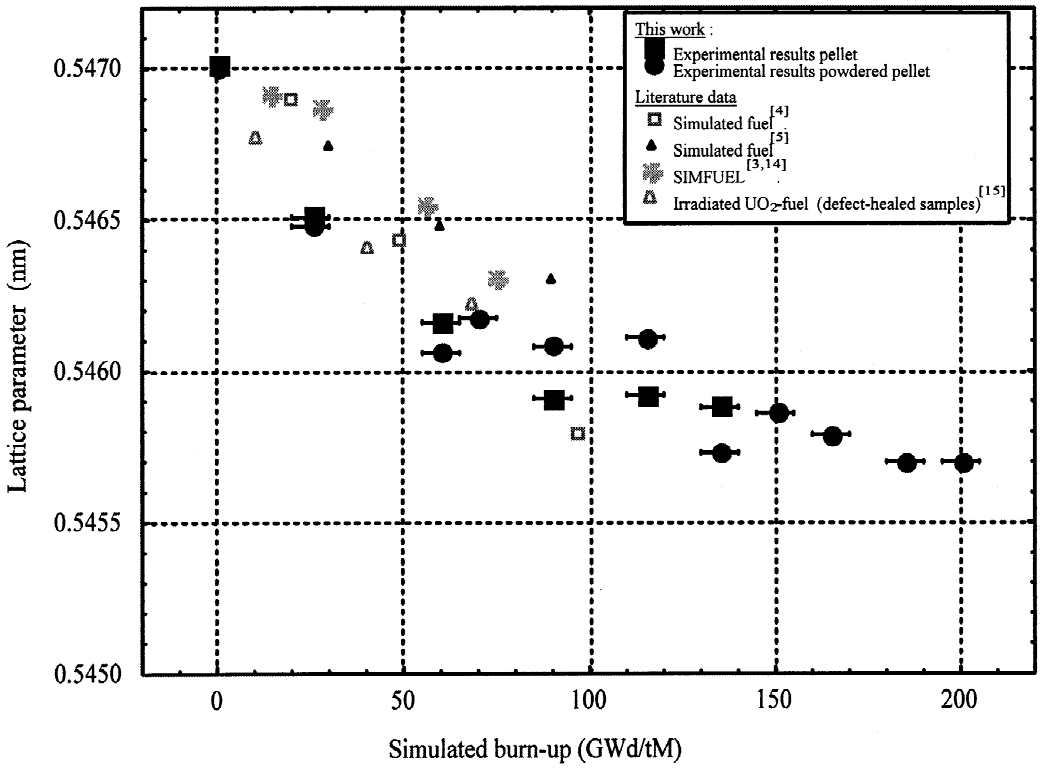

Fig. 1. Lattice parameter of simulated spent fuels as a function of the burn-up.

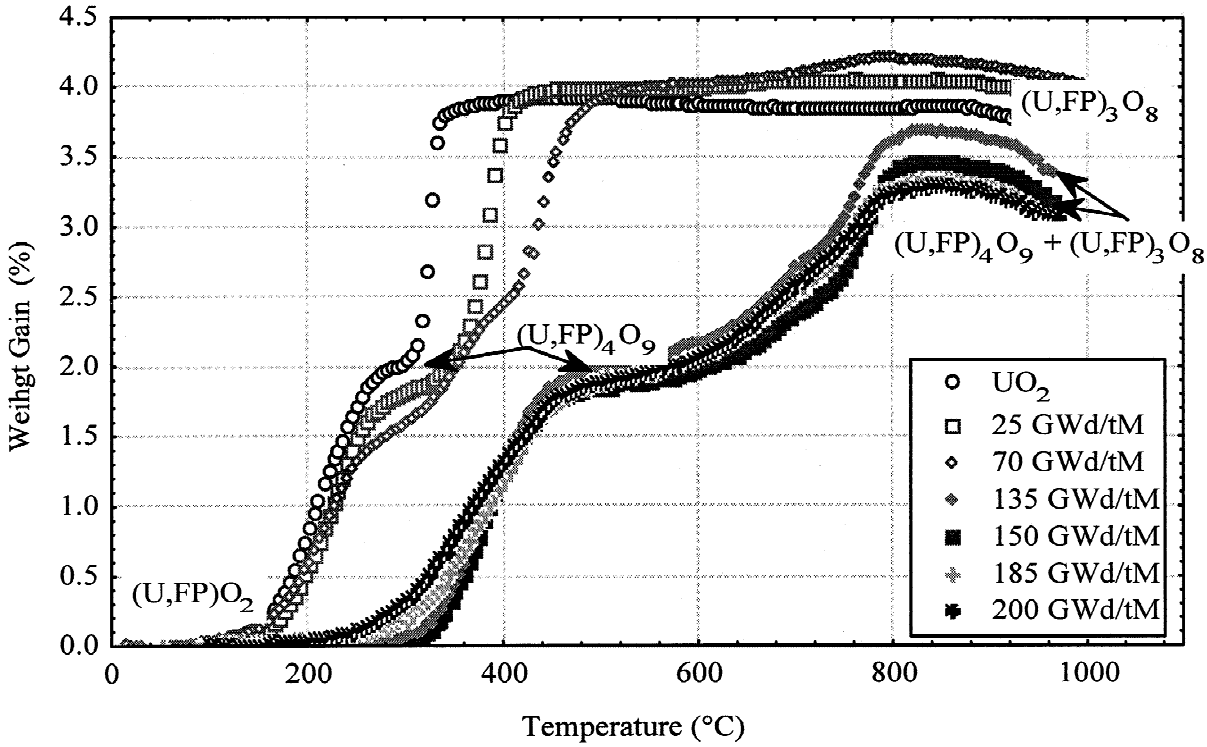

Fig. 2. Oxidation kinetics of unirradiated UO_2 and simulated spent fuels. Starting material: powdered pellets (mesh #220).

X-ray results show no complete transformation to the (U, FP)$_3$O$_8$ structure even up to the highest temperatures examined, while important fractions of the (U, FP)$_4$O$_9$ still remain up to these high temperatures.

The curves show in general a delayed oxidation kinetic as the concentration of simulated fission products (FP) increases (Fig. 2). The strongest effect is observed above 70 GWd tM^{-1}, where the steepest increase in the transformation temperatures to the (U, FP)$_4$O$_9$ and (U, FP)$_3$O$_8$ phases is noticed (Fig. 2).

Since the molecular weight of the oxide decreases as uranium is replaced by lighter atoms, the same oxidation level (O/M ratio) demands higher relative weight changes as burn-up increases. This is clearly seen in the curves of Fig. 2 up to burn-ups of 70 GWd tM^{-1}. For higher burn-ups, however, progressively lower weight-gains at maximum temperatures are observed (Fig. 2). Two reasons can be argued for this behaviour, namely lower saturating O/M ratios, or higher evaporation rate of the (U, FP)$_3$O$_8$ phase.

3.3.2. Bulk pellets

Fig. 3 shows typical oxidation curves of bulk sintered-pellets of UO_2 and simulated fuels. Compared to the curves of Fig. 2 (powdered pellets), the same qualitative behaviour is observed, with the only difference, that in the low burn-up range (<90 GWd tM^{-1}) one-step oxidation from (U, PF)O$_2$ to (U, FP)$_3$O$_8$ is noticed (Fig. 3). This kind of one-step oxidation curve is characteristic of pure UO_2 in the form of pellets and coarse powders [18].

At burn-ups of 115 GWd tM^{-1} and above, a two-step oxidation curve ((U, FP)O$_2$→(U, FP)$_4$O$_9$→(U, FP)$_3$O$_8$), as for the samples of Section 3.3.1, was observed. It is worth noting that at these high burn-ups, the fully oxidised samples never did transform to powder, as would be expected from a complete transformation to the less dense phase (U, FP)$_3$O$_8$. As a confirmation, the X-ray diffraction analysis of the fully oxidised pellet-samples at high burn-ups, always showed large remaining fractions of the (U, FP)$_4$O$_9$ phase.

4. Discussion and conclusions

The present results show that as far as the dissolution of fission products is concerned, the burn-up increase causes a continuous decrease of the UO_2-lattice parameter. As mentioned in Section 3.2, the observed trend in our results is in good agreement with pre-existing data [3–5,14,15], especially if values above 90 GWd tM^{-1} are considered (Fig. 1). At lower burnups, however, lower lattice constants were measured in our case with respect to earlier results (Fig. 1). This trend is attributed to a probable contamination of our material with Zr and Y (Section 3.1), due to the use of zirconia–yttria balls and container during the milling operation. It is known that among all fission products soluble in UO_2, the largest lattice contraction is caused by Zr. At larger burnups, the effect of this

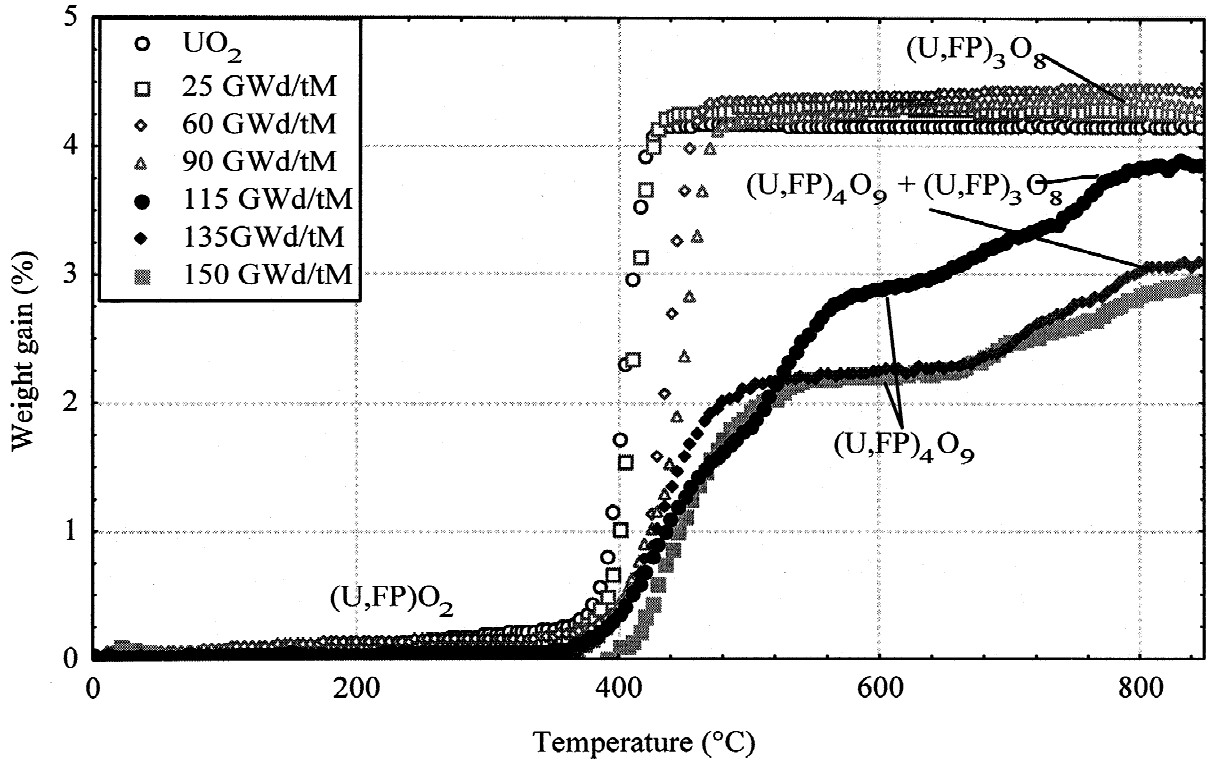

Fig. 3. Oxidation kinetics of unirradiated UO_2 and simulated spent fuels. Starting material: Bulk sintered pellets.

contamination becomes relatively less important, because much higher amounts of dopants are used (Table 1).

With respect to the oxidation behaviour of the simulated spent fuel samples (Figs. 1 and 2), the present results show that up to the highest temperatures examined (950–1000°C), a marked delay of the transformations to the (U, FP)$_4$O$_9$ and (U, FP)$_3$O$_8$ phases and an enlarged temperature range of existence of the phase (U, FP)$_4$O$_9$ is observed. These results fully agree with the suggestion [8] that the U_4O_9-phase may be stabilised by dissolved fission products when the irradiated fuel is oxidised at low temperatures. Also, the observed delay in the transformation to (U, FP)$_4$O$_9$ (Figs. 2 and 3) is in agreement with recent results of specific heat measurements on stoichiometric and hyperstoichiometric UO_2 and SIMFUEL, showing the absence of (U, FP)$_4$O$_9$ formation in slightly hyperstoichiometric SIMFUEL samples, in contrast to UO_2 [19]. The techniques used were X-ray diffraction [19] and the coulometric titration technique [20].

As a conclusion, the present results indicate that the formation of the deleterious (U, FP)$_3$O$_8$ phase (due to its volume increase), in the case of the irradiated fuel subjected to accidental leaks, may be strongly delayed when the local burn-up of the exposed zone, usually the fuel-rim, is over 80–100 GWd tM^{-1}. Further detailed studies about the width of the (U, FP)$_4$O$_9$ phase field as a function of temperature and oxygen potential seem to be still necessary.

Acknowledgements

The authors thank G. Nicolaou for the ORIGEN calculations. C. Fuchs for sample preparations, F. Rousseu for optical microscopy determinations are also deeply appreciated.

References

[1] H. Kleykamp, J. Nucl. Mater. 131 (1985) 221.
[2] H. Kleykamp, J. Nucl. Mater. 84 (1979) 109.
[3] P.G. Lucuta, Hj. Matzke, R.A. Verrall, B.J. Palmer, J. Nucl. Mater. 178 (1991) 48.
[4] K. Une, Y. Tominaga, S. Kashibe, J. Nucl. Sci. Tech. 28(5) (1991) 409.
[5] S. Ishimoto, M. Hirai, K. Ito, Y. Korei, J. Nucl. Sci. Tech. 31(8) (1994) 796.
[6] K. Laßmann, C. O'Carroll, J. van de Laar, C.T. Walker, J. Nucl. Mater. 231 (1996) 179.
[7] J. Spino, F. Montigny, unpublished results.
[8] L.E. Thomas, R.E. Einziger, H.C. Buchanan, J. Nucl. Mater. 201 (1993) 310.
[9] J.W. Choi, R.J. McEachern, P. Taylor, D.D. Wood, J. Nucl. Mater. 230 (1996) 250.
[10] A.G. Croff, ORNL-5621 UC-70, 1980.
[11] Seifert XDAL 3000 Software, Revision 1.4, June 11, 1993.
[12] F. Schmitz, G. Dean, M. Halachmy, J. Nucl. Mater. 40 (1971) 325.
[13] Gmelin Handbook of Inorganic Chemistry, Suppl. vol. C4 Uranium dioxide, D. Vollath, H. Wedemeyer, R. Keim, C. Keller (Eds), Springer-Verlag, Berlin, 1984.

[14] P.G. Lucuta, B.J. Palmer, Hj. Matzke, D.S. Hartwig, Report AECL-10117, 1989.
[15] J.H. Davies, F.T. Ewart, J. Nucl. Mater. 41 (1971) 143.
[16] N. Masaki, J. Nucl. Mater. 101 (1981) 229.
[17] S.R. Teixeira, K. Imakuma, J. Nucl. Mater. 178 (1991) 33.
[18] K.T. Scott, K.T. Harrison, J. Nucl. Mater. 8(3) (1963) 307.
[19] Hj. Matzke, P.G. Lucuta, R.A. Verrall, J. Henderson, J. Nucl. Mater. 247 (1997) 121.
[20] P.G. Lucuta, Hj. Matzke, D.S. Cox, Proceedings of the International Symposium on the Thermodynamics of Nuclear Material, Osaka, Aug. 25–30, 1996.